Investigation of the Thermoelectric Properties of Metal Chalcogenides with SnSe

Undergraduate Researcher
Katherine R. Stevens
Carthage College, Kenosha, WI

Faculty Mentor
Mercouri G. Kanatzidis
Department of Chemistry
Northwestern University

Postdoctoral Mentor
Simon Johnsen
Department of Chemistry
Northwestern University

Graduate Student Mentor
Steven N. Girard
Department of Chemistry
Northwestern University

Abstract

Thermoelectric materials, which convert heat energy to electrical energy, may become increasingly important in the world's energy situation. Through the inclusion of nanoscale features embedded within a thermoelectric bulk material, it has been shown that a corresponding decrease in lattice thermal conductivity results in an enhanced thermoelectric figure of merit, ZT. This project focused on a new method of nanostructuring: lowering the lattice thermal conductivity by generating a two-phase material in which one phase had nanoscale layers to scatter phonons. The thermoelectric properties of metal chalcogenides with SnSe were investigated for three systems: PbTe-SnSe, PbSe-SnSe, and SnTe-SnSe. PbTe-SnSe formed a solid solution with decreased thermal conductivity over PbTe but poor ZT. PbSe-SnSe and SnTe-SnSe formed multiphase systems with significantly decreased thermal conductivities compared to their parent materials at room temperature (maximum 26.2% and 87%, respectively). In addition, SnTe-SnSe showed promise for further research because it is naturally p-type, less toxic than lead-based materials, and showed a maximum ZT of 0.45 at 700K for a SnTe-SnSe 20% sample.

Introduction

As the world energy crisis intensifies, technologies that operate efficiently and with little to no CO_2 emissions are becoming increasingly important. Thermoelectric (TE) materials, solid-state materials that convert heat energy to electricity and vice versa, address both of these issues. They are capable of scavenging and converting waste heat generated by other power generation methods. Additionally, these solid-state materials have no moving parts, operate quietly, and require little to no maintenance. These advantages have made them viable for a variety of applications including military imaging systems for heat-seeking missiles and night vision, medical instruments, car-seat temperature regulators, and deep-space NASA probes.[1–3]

TE materials are capable of energy conversion by the Seebeck effect, where a temperature gradient across a material induces a voltage according to

$$S = \frac{\Delta V}{\Delta T}$$

where S is the Seebeck coefficient. The inverse process, the Peltier effect, allows a current to create a temperature gradient in the material, which is useful for heating and cooling applications. Despite their advantages, TE applications have been limited because their energy-conversion efficiency is low. Many modern devices run with efficiencies of 5–6%, which is not cost effective for large-scale commercialization. Thus, current research in TE materials deals mainly with improving existing materials and discovering new systems to get the greatest efficiency possible.[4] TE performance depends both on the temperature gradient across the material (ΔT) and on the figure of merit, ZT:

$$ZT = \frac{S^2 \sigma T}{\kappa_{tot}}$$

where σ is the electrical conductivity, T is the temperature, and κ_{tot} is the total thermal conductivity. κ_{tot} is a combination of the thermal energy transported by charge carriers (κ_{el}) and the lattice thermal energy transported by phonons (κ_{latt}). The electrical transport $S^2\sigma$ term is called the power factor. The ZT of a material changes with temperature so TE materials in use today are optimized for specific temperature regions where their ZT values are the highest. Bi_2Te_3 is often used at room temperature, PbTe is used at 600–700 K, and SiGe is used at 1200 K. Each of these materials has a ZT of about 0.8–1.0 in its optimal temperature range.[4] Power-generation efficiency is calculated by combining the Carnot efficiency and ZT_{avg} (Figure 1).

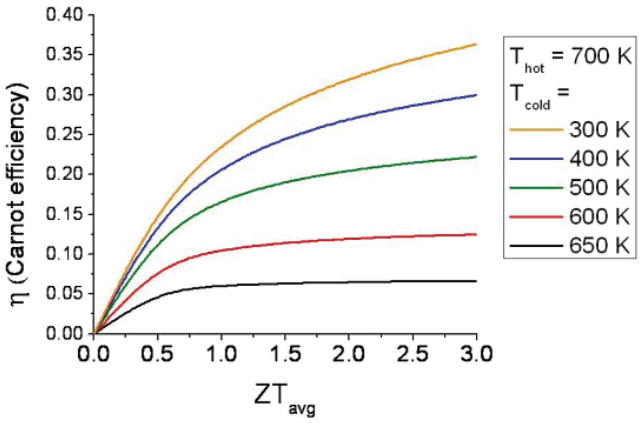

Figure 1. TE energy conversion efficiency (η) vs. ZT_{avg}. Many modern materials operate at 5–6% efficiency, but it is predicted that much higher efficiencies are possible.[4]

A high ZT can be obtained by increasing the power factor and decreasing κ_{tot}. However, this can often be difficult because all of the properties except κ_{latt} are dependent on the electronic structure of the material. The S and σ variables are inversely coupled (so an increase in σ will result in a decrease in S, and vice versa), and σ and κ_{el} are directly coupled. In response to this inherent materials conflict, TE research has moved forward in two directions: (1) decoupling S and σ to increase the power factor and (2) reducing κ_{latt}.[3]

Much research has focused on reducing κ_{latt} through nanostructuring. Phonons, the heat-carrying quantum particles that contribute to κ_{latt}, have a range of wavelengths and mean free paths depending on temperature but are often on the order of about 1–100 nm.[5] The mean free paths of electrons are generally smaller at the same temperatures, so nanoscale interfaces inside the materials scatter phonons more effectively than electrons.[3] Approaches include making thin-film multilayers and quantum-dot superlattices for enhanced acoustic phonon scattering. Although these techniques have resulted in ZTs greater than 2, they are often expensive in addition to having difficulties associated with scale-up.[6–8]

Nanostructuring of bulk TE materials has received considerable attention recently. In this top-down technique, a nanoscale second phase is generated inside a bulk material that has already shown good TE performance by taking advantage of inherent material properties, such as phase immiscibility.[9] Nanostructures contribute to phonon scattering to reduce κ_{latt} and increase ZT.[3] This approach is attractive because of its comparatively low cost and potential for scale-up in industry.

Background

Optimally doped PbTe has a ZT of 0.8–1.0 at ~650 K and has been considered for several midrange (600–800 K) temperature applications, but a higher ZT is needed for wide-scale utilization. It has been shown that the TE properties of PbTe can be improved by nanostructuring, mainly by lowering κ_{latt}.[4] Several high-ZT nanostructured PbTe materials are shown in Figure 2.[10] The LAST-m system ($AgPb_mSbTe_{2+m}$), with a ZT of ~1.7 at 700 K, was the first bulk nanostructured PbTe-based material to be discovered. Nanostructures spontaneously formed upon cooling from the melt but the TE properties proved to be extremely sensitive to cooling conditions due to the material's complex phase diagram.[11] Its p-type analogue, LASTT, has a reported ZT of ~1.4 at 700 K.[12] In 2007, PbS nanoparticles were formed in PbTe by taking advantage of a miscibility gap to create natural nanostructuring. PbTe-PbS 8% exhibited a ZT of 1.5 at 650 K.[4,13] In another study co-nanostructuring of PbTe with Pb and Sb precipitates through matrix encapsulation resulted in a ZT of 1.4 at 673 K.[4,14] Although these bulk approaches have resulted in high ZTs, the conditions used to obtain them do not apply to every TE system. For this reason, other bulk nanostructuring methods should be investigated.

Approach

This research investigated the combination of PbTe and other metal chalcogenides with SnSe. SnSe forms a Pnma orthorhombic crystal structure (Figure 3; lattice parameters a=1.1501 nm, b=0.4153 nm, c=0.4445 nm)[15] that has inherent layering on the nanoscale. Combining this Pnma crystal structure with the cubic Fm3m structure of PbTe could potentially yield interesting TE properties. It was suspected that inherent layering within the Pnma crystal structure could scatter phonons and decrease κ_{latt}.

While PbTe has been studied extensively as a TE material, it has some disadvantages, such as the toxicity of lead and the high cost of tellurium. SnTe and PbSe belong to the cubic Fm3m space group and may exhibit interesting TE properties. Therefore, they were investigated in addition to PbTe.

Pb, Sn, Te, and Se (99.99% purity) were reacted to generate the stock materials PbTe, PbSe, SnTe, and SnSe. Samples were flame-sealed in quartz ampoules under a vacuum of 10^{-4} torr. The combined binaries were reacted for about 6 hr at temperatures from 970 to 1100° C as dictated by their phase diagrams. All samples were then shaken to ensure good mixing and then rapidly cooled.

Samples were characterized for structure by scanning electron microscopy (SEM; Hitachi S3400) and powder x-ray diffraction (PXRD; Inel CPS-120). Chemical composition was verified in selected SEM samples by energy dispersive spectroscopy (EDS).

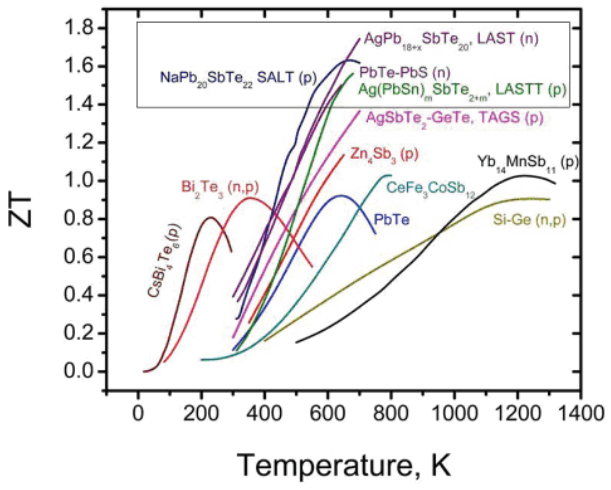

Figure 2. High-ZT materials including nanostructured materials based on PbTe: LAST-m, LASTT, SALT, and PbTe-PbS.[8]

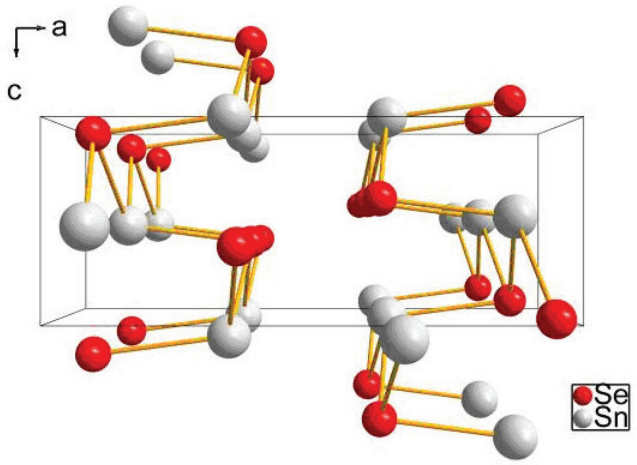

Figure 3. Pnma crystal structure of SnSe. The inherent layering in the structure may contribute to enhanced phonon scattering for a low κ_{latt} value.

Electrical properties measurements were performed on a ULVAC ZEM-3. A sample of average dimension 2 x 2 x 8 mm was mounted between two nickel electrodes. Two k-type thermocouples provided forced probe contacts to one face of the sample. The Seebeck coefficient and electrical resistivity were measured simultaneously from 300 to 700 K.

Thermal conductivity measurements were performed on a Netzsch LFA-457. Sample coins with an average dimension of 8 mm diameter and 2 mm thickness were coated with graphite and then irradiated with HeNe pulsed-laser light. The corresponding temperature change of the opposite side was measured by an IR detector to determine thermal diffusivity (κ_{diff}). κ_{tot} was calculated according to $\kappa_{tot} = \rho C_p \kappa_{diff}$ where ρ is the density of the sample measured from sample dimensions and mass and C_p is the specific heat calculated according to a Pyroceram 9606 reference. The material was assumed to have a linear expansion coefficient. κ_{el} was calculated using the Wiedemann-Franz law: $\kappa_{el} = L_0 \sigma T$ where $L_0 = 2.45 \times 10^{-8}\ J^2K^{-2}C^{-2}$ for free electrons.[3] κ_{el} was subtracted from κ_{tot} to obtain κ_{latt}.

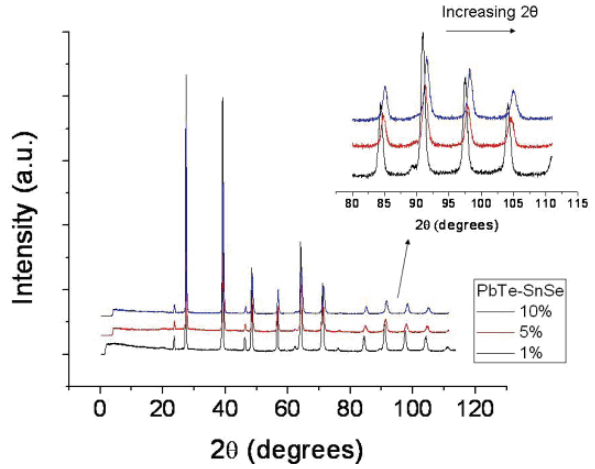

Figure 4. PXRD analysis showing solid-solution alloying of PbTe-SnSe system in 1%, 5%, and 10% SnSe samples. The PXRD exhibits clear PbTe peaks that shift to higher 2θ values with increasing SnSe concentrations (inset). This shift is consistent with shorter lattice parameters caused by Sn and Se insertion into the PbTe crystal lattice. SEM analysis of PbTe-SnSe samples confirms solid-solution alloying with the presence of one homogenous phase.

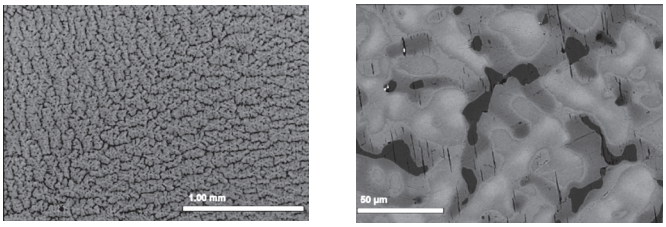

Figure 5. SEM images of PbSn-SnSe 50% sample. PbSe-SnSe forms a multiphase system with regions of varying SnSe concentrations. The darker areas are SnSe rich and the brighter areas are PbSe rich. It was suspected that multiple phases could lead to decreased κ_{latt} values.

Results

PbTe-SnSe System

As of the publication of this work, the PbTe-SnSe system has not been explored for either phase relations or TE properties. PXRD of synthesized samples of PbTe-SnSe 1%, 5%, and 10% are shown in Figure 4. Each peak can be indexed as belonging to the PbTe cubic phase without any presence of orthorhombic SnSe. A corresponding shift to higher 2θ with increasing SnSe concentration suggests the creation of a solid-solution alloy whose lattice parameter is monotonically decreased as Sn and Se are substituted for Pb and Te within the matrix (Figure 4 inset). It is well understood that PbTe will form solid-solution alloys with both PbSe and SnTe;[16,17] it would appear that the PbTe-SnSe system preferentially behaves the same way: PbTe + SnSe → $Pb_{1-x}Sn_xTe_{1-y}Se_y$

PbSe-SnSe System

According to the PbSe-SnSe phase diagram, a two-phase system exists between 46% and 78% SnSe at 400 K.[18] Samples of PbSe-SnSe 40% and 50% were synthesized to target the two-phase region of phase immiscibility in this system. Samples were doped n-type with 0.055% $PbCl_2$.

SEM images show a multiphase system with areas of varying SnSe concentration (Figure 5). The bright areas are PbSe rich and the dark are SnSe rich, but complete phase separation was not observed. PXRD (Figure 6) displays peaks indexed for both PbSe and SnSe crystal structures with slight shifts in 2θ indicating some solid-solution alloying:

$Pb_{1-x}Sn_xSe + Sn_{1-y}Pb_ySe$

Fm3m Pnma

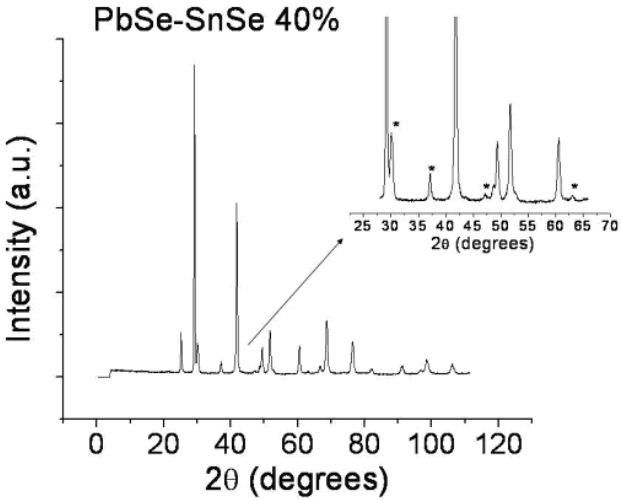

Figure 6. PXRD of the PbSe-SnSe 40% sample shows peaks consistent with PbSe and SnSe (inset: * indicates SnSe peak).

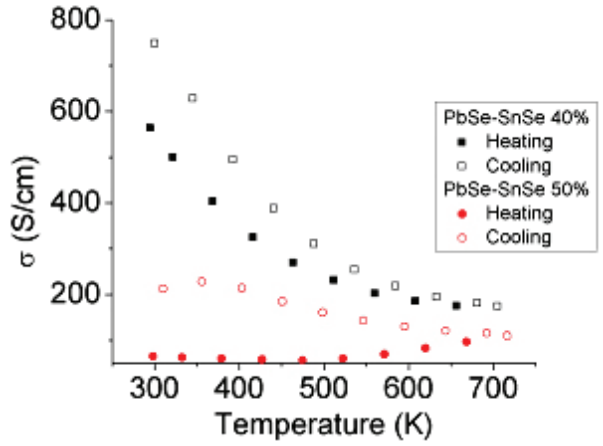

Figure 7A

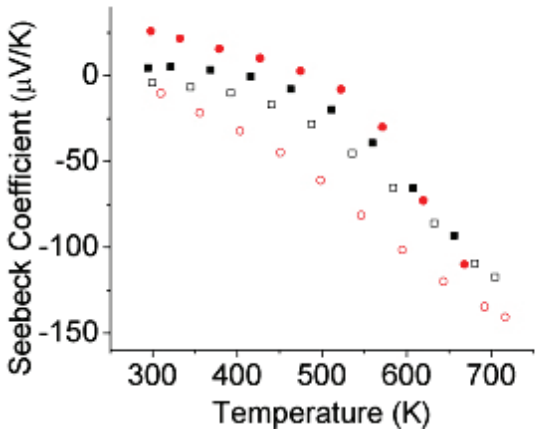

Figure 7B

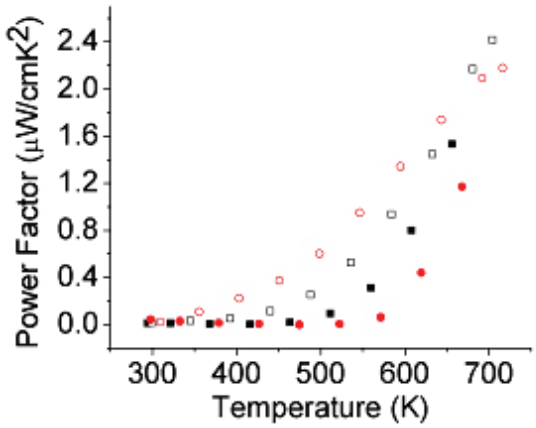

Figure 7C

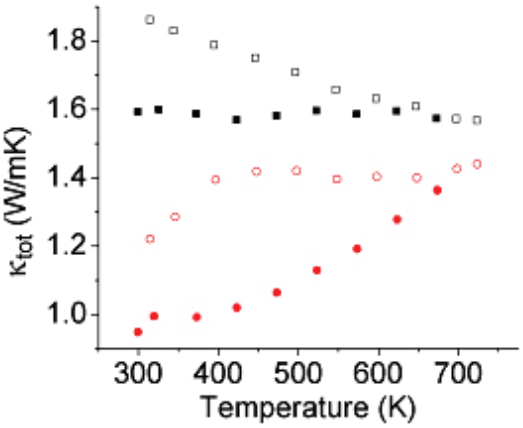

Figure 7D

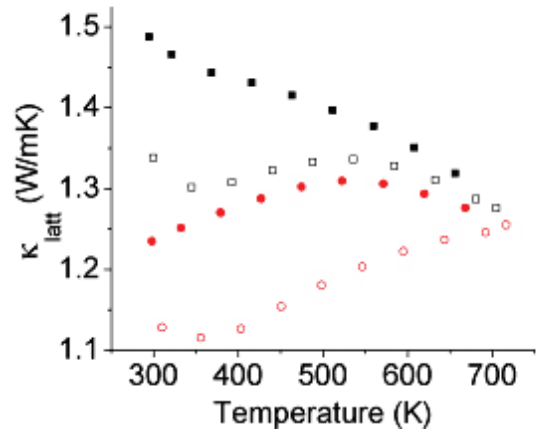

Figure 7E

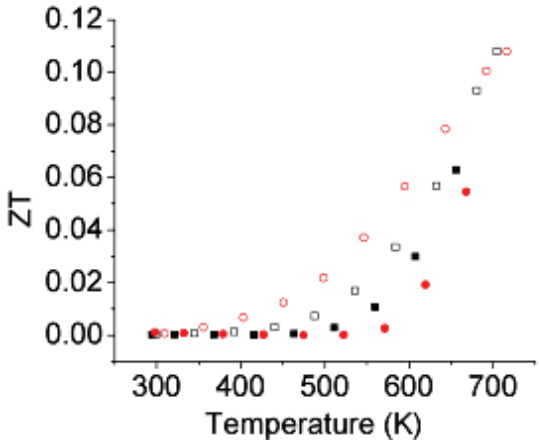

Figure 7F

Figure 7. TE properties of PbSe-SnSe. The total thermal conductivity of the PbSe-SnSe 50% sample is lower than that of PbSe, but PbSe-SnSe 40% is higher. Samples showed instability upon heating and cooling during measurement, possibly due to annealing of cracks and movement of phases to thermodynamic equilibrium.

The TE properties for PbSe-SnSe samples are shown in Figure 7. Some instability is evident in each of the properties measurements; this is possibly due to the annealing of cracks in the sample, visible in the SEM images at 50 μm. It may also be that the rapidly cooled samples were not allowed to reach thermodynamic equilibrium. In the future, it is recommended that samples be annealed prior to TE properties measurements to increase stability.

At 323 K, PbSe has a κ_{tot} of 1.625 W/mK.[19] The PbSe-SnSe 50% sample shows a κ_{tot} of ~1.2 at the same temperature, a decrease of 26% (Figure 7e). At 40% SnSe, κ_{tot} actually increased over PbSe alone. For both samples, the ZT of this material at all temperatures remained low (<0.12).

SnTe-SnSe System

The phase diagram for the SnTe-SnSe system suggests that a two-phase system forms for SnSe concentrations of 28–74% at 400 K.[20] Samples of SnTe-SnSe 20%, 30%, and 40% were synthesized to target the two-phase/solid-solution boundary in the phase diagram. PXRD shows a two-phase system with clear SnTe and SnSe peaks (Figure 8). As the concentration of SnSe was increased, the SnTe peaks shifted to higher 2θ values, indicating some solid-solution alloying behavior. Likewise, the SEM reveals two phases: the dark regions are SnSe rich and the bright regions are SnTe rich (Figure 9). Cracks of 1–5 μm in length and ~100 nm in width formed preferentially in the SnTe phase. In general, cracks reduce electron mobility and electrical contact between grains, so further synthesis optimization could be performed.

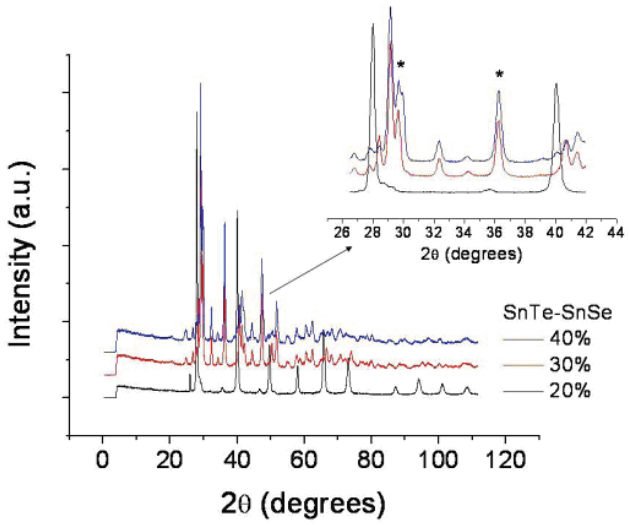

Figure 8. PXRD for SnTe-SnSe 20%, 30%, and 40% samples. Nearly every peak for the 20% sample can be indexed by cubic SnTe (20% SnSe lies in the solid-solution portion of the phase diagram). As the SnSe concentration is increased, distinct SnSe peaks become more prominent (* in inset).

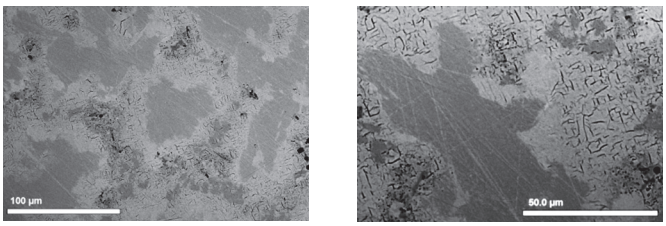

Figure 9. SEM images of a SnTe-SnSe 33% sample. Two phases are shown, each mixtures of SnTe and SnSe. The darkest areas are SnSe rich and lightest areas are SnTe rich. Cracks of ~5 μm by 100 nm form preferentially in the SnTe-rich regions.

Initial samples ranging from 20–46% SnSe showed large instability upon heating and cooling during measurement. Subsequent SnTe-SnSe 20%, 30%, and 40% samples were annealed at 500°C for 36 hours prior to TE properties measurements, shown in Figure 10. All samples were naturally p-type and exhibited very low κtot for a SnTe-based system. SnTe has a κ_{tot} of 7.9 W/mK at room temperature while the SnTe-SnSe 40% sample showed a κ_{tot} of ~1.0 W/mK at the same temperature, an 87% decrease.[21] As the concentration of SnSe increased, σ decreased while S stayed relatively constant. This contributed to a higher power factor for the SnTe-SnSe 20% sample. A maximum ZT of 0.45 at 700 K was obtained for the SnTe-SnSe 40% sample. This ZT could be increased by tuning the charge-carrier concentration since the current S is limited by a high σ value.

Discussion

It was expected that the inclusion of SnSe into metal chalcogenide systems would result in a two-phase material with good electrical and thermal transport properties contributing to a high ZT. PbTe-SnSe formed a solid solution for concentrations from 1–10% SnSe, appeared naturally undoped, and therefore was not considered for properties analysis.

The PbSe-SnSe system formed a multiphase material with SnSe-rich and PbSe-rich regions but no complete phase separation. The TE properties of samples of PbSe-SnSe 40% and 50% were not very promising, with a maximum ZT of 0.12 at 700 K for the 50% sample. This is mostly due to low power factors and high thermal conductivities.

SnTe-SnSe formed a successful two-phase system, although it exhibited some solid-solution behavior. This system is especially interesting because all samples were naturally p-type and contained no lead, leading to lower toxicity. In addition, samples showed a large reduction in κ_{tot} (an 87% decrease at room temperature for the SnTe-SnSe 40% sample). The electrical properties of this system showed some interesting trends: σ decreased significantly with increasing SnSe while S remained relatively unchanged. σ can be defined by $\sigma = ne\mu$ where n is the number of charge carriers, e is the fundamental charge of an electron, and μ is charge carrier mobility. The stability of the σ values indicates that n stayed constant, so it may be that μ changes with SnSe concentration. The SnTe-SnSe 20% sample showed a high power factor of ~12 at 700 K, leading to a ZT of 0.45 at the same temperature. Charge carrier optimization may prove useful to increase these values.

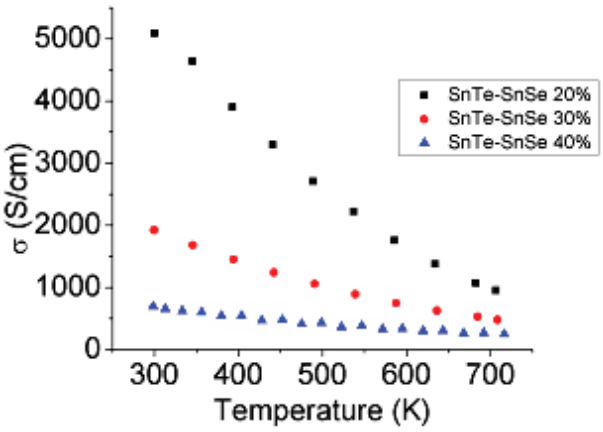

Figure 10A

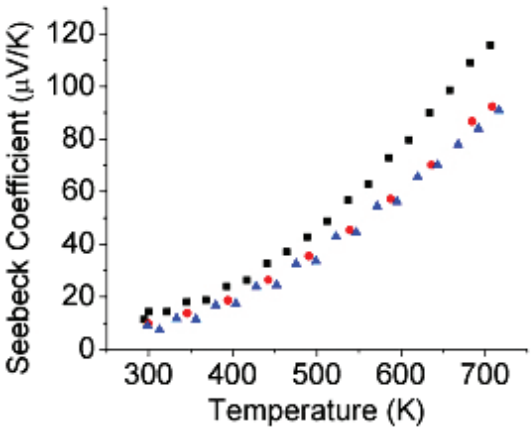

Figure 10B

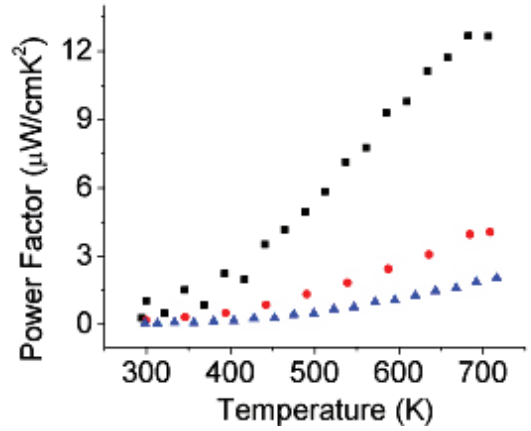

Figure 10C

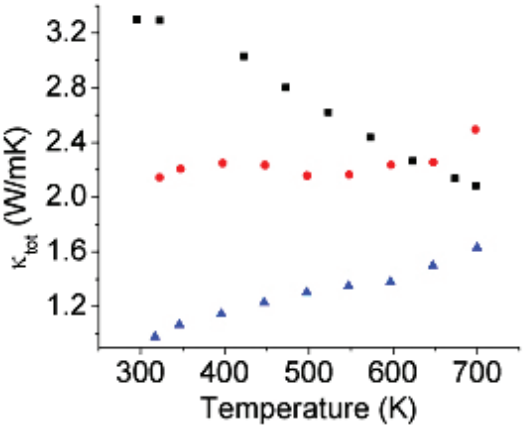

Figure 10D

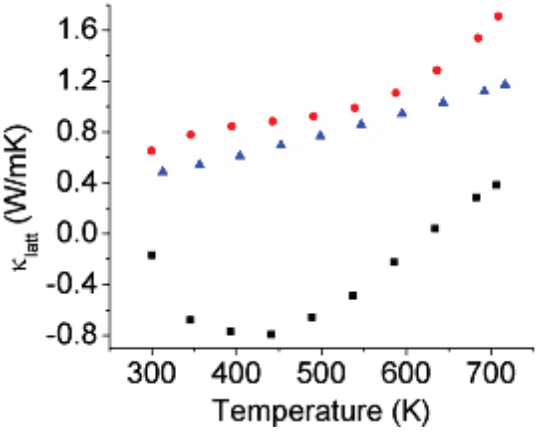

Figure 10E

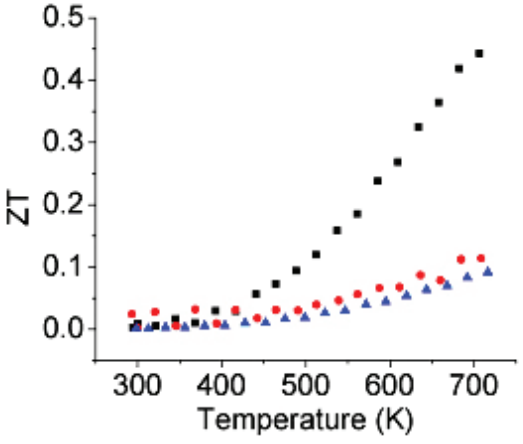

Figure 10F

Figure 10. Electrical transport and ZT for SnTe-SnSe 20%, 30%, and 40% undoped samples after annealing. Natural p-type character leads to high σ and a low S. This limits the power factor and the ZT of the material, although a high ZT of 0.45 is still obtained for the SnTe-SnSe 20% sample at 700 K. The thermal conductivity of the SnTe-SnSe 40% sample is 87% lower than SnTe at room temperature.

Conclusions

This project investigated the TE properties of PbTe-SnSe, PbSe-SnSe, and SnTe-SnSe systems. PbTe-SnSe appeared to form a solid solution, while the PbSe-SnSe and SnTe-SnSe systems formed multiphase materials. PbSe-SnSe demonstrated poor TE properties (ZT_{max} ~0.12 at 700 K) but could potentially be optimized by further doping. SnTe-SnSe was a very promising system that showed natural p-type character, low κ_{tot} compared to SnTe, and a maximum ZT of 0.45 at 700 K for the SnTe-SnSe 40% sample. This system could be further optimized with heat treatment, SnSe concentration, and doping studies.

This research was supported primarily by the Northwestern University Nanoscale Science and Engineering Research Experience for Undergraduates (REU) Program under National Science Foundation (NSF) award number ***EEC – 0755375.*** *Any opinions, findings, conclusions or recommendations expressed in this material are those of the author(s) and do not necessarily reflect those of the NSF.*

References

1 Bell, L. E. *Science* **2008,** *321,* 1457–1461.
2 Tritt, T. M.; Subramanian, M. A. *MRS Bull.* **2006**, *31,* 188–194.
3 Snyder, G. J.; Toberer, E. S. *Nat. Mater.* **2008**, *7,* 105–114.
4 Sootsman, J. R.; Chung, D. Y.; Kanatzidis, M. G. *Angew. Chem. Int. Ed.* **2009**, in press.
5 Dames, C. C. "Thermal Conductivity of Nanostructured Thermoelectric Materials." In Rowe, D.M., ed., *Thermoelectrics Handbook Macro to Nano.* Boca Raton: CRC Press, **2006**.
6 Poudel, B., et al. *Science* **2008**, *320,* 634–638.
7 Venkatasubramanian, R., et al. *Nature* **2001**, *413,* 597–602.
8 Harman, T. C., et al. *Science* **2002**, *297,* 2229–2232.
9 Ikeda, T., et al. *Chem. Mater.* **2007**, *19,* 763–767.
10 Sootsman, J. R., http://chemgroups.northwestern.edu/kanatzidis/index.html. *Kanatzidis Research Group*, **2009**.
11 Hsu, K. F., et al. *Science* **2004**, 303, 818–821.
12 Androulakis, J., et al. *Adv. Mater.* **2006**, *18*, 1170.
13 Androulakis, J., et al. *J. Am. Chem. Soc.* **2007**, *129*, 9780–9788.
14 Sootsman, J. R., et al. *Angew Chem. Int. Ed.* **2008**, *47*, 8618–8622.
15 Chattopadhyay, T.; Pannetier, J.; Vonschnering, H. G. *J. Phys. Chem. Solids* **1986**, *47*, 879–885.
16 Elaguina, E. I.; Abrikosov, N. K. *Dokl. Akad. Nauk* **1956**, *111,* 353–354.
17 Abrikosov, N. K.; Dyuldina, K. A.; Danilyan, T. A. *Zh. Neorg. Khim.* **1958**, *3,* 1632–1636.